On the dissipation mechanism of lattice Boltzmann method when modeling 1-d and 2-d water hammer flows[☆]

Moez Louati [a,*], Mohamed Mahdi Tekitek [b], Mohamed Salah Ghidaoui [a]

[a] Department of Civil and Environmental Engineering, The Hong Kong University of Science and Technology, Hong Kong
[b] Department of Mathematics, Faculty of Science of Tunis, University of Tunis El Manar, Tunis 2092, Tunisia

ARTICLE INFO

ABSTRACT

This paper uses the multiple relaxation times lattice Boltzmann method (LBM) to model acoustic wave propagation in water-filled conduits (*i.e.* water hammer applications). The LBM scheme is validated by solving some classical water hammer (WH) numerical tests in one-dimensional and two-dimensional cases. In addition, this work discusses the accuracy, stability and robustness of LBM when solving high frequency (*i.e.* radial modes are excited) acoustic waves in water-filled pipes. The results are compared with a high order finite volume scheme based on Riemann Solver. The results show that LBM is capable to model WH applications with high accuracy and performance at low frequency cases; however, it loses stability and performance for high frequency (HF) cases. It is discussed that this is due to the neglected high order terms of the equivalent macroscopic equations considered for LB numerical formulation.

1. Introduction

Waves are used as diagnostic tools for imaging and defect detection in a wide range of science and engineering applications (*e.g.* medicine, oceanography, materials and many others. In particular, acoustic waves are used in sonography (echography in medicine) and ocean topography identification. Current work in hydraulic (engineering) research uses acoustic waves for defect detection in water supply systems (e.g. [10,21,26,28]). More recently, attempts are being made to spatially locate and identify defects at high resolution using high frequency waves (HFW). However, the use of high frequency probing waves (HFW) excites radial and azimuthal wave modes in pipe systems, making classical one-dimensional water hammer (WH) theory incapable of solving the hydraulic problem.

To conserve the physical dispersion behavior of HFW, dispersive numerical schemes (e.g. [23–25]) should be avoided. Louati and Ghidaoui [25] showed that a 2nd order FV scheme performs poorly for modeling HFW and high order schemes are required to reduce numerical dispersion effects. Louati and Ghidaoui [23,24] used a fifth order numerical scheme based on a Riemann solver with

WENO reconstruction to model and study the behavior of HFW in a simple pipe system. However, because of complex boundary conditions needed in hydraulic engineering (e.g., pumps, pressure relief valves, pressure reducing valves, and so on), it is best to avoid the use of high order schemes due to the increased mathematical and numerical difficulty of implementing the boundary conditions. The lattice Boltzmann method (LBM) is a popular alternative to high order schemes and is known for its excellent performance in engineering applications. For this reason, this paper studies the efficiency of the LBM to model water hammer flows and high frequency waves. In fact, LBM makes it possible to simulate various types of fluid flows with simple algorithms (see e.g. [5,9,20,31,32]). In simple cases, second order accuracy can be easily verified (see e.g. [19]). As the LBM needs only nearest neighbor information to achieve a solution, the algorithm is an ideal candidate for parallel computing. These features make the LBM increasingly popular for engineering applications. Currently, the LBM is a well-known computational fluid dynamics method that models flow in a way that is consistent with formal solutions of viscous and incompressible Navier-Stokes equations [29]. However, use of the LBM for acoustics (compressible flow) applications is fairly recent and its utility and performance characteristics are not yet well known.

LBM was first used by Buick et al. [2] to simulate sound waves (at low frequency) in situations where fluid density variation is small compared with mean density. Dellar [8] studied the ability of the LB scheme to model sound waves and investigated the influence on the numerical scheme of bulk viscosity and shear viscos-
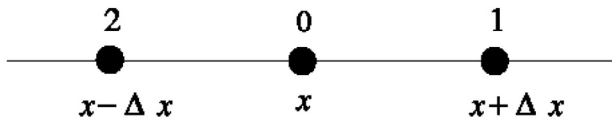
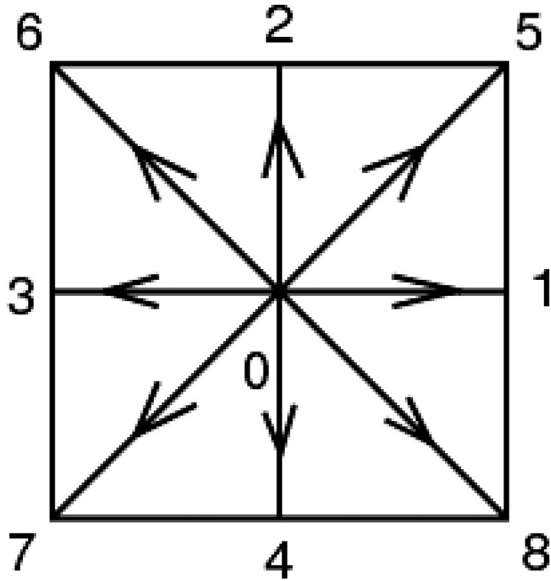**Fig. 1.** Stencil for the D1Q3 lattice Boltzmann scheme.

Fig. 2. Stencil for the D2Q9 lattice Boltzmann scheme.

ity. Course et al. [7] used LBM to investigate four canonical acoustic problems involving traveling and standing acoustic waves and showed the capability of the LBM to reproduce fundamental acoustic wave phenomena.

Recently Marié et al. [27] showed that dispersion error of acoustic waves in lattice Boltzmann models is due to effects of space and time discretization. They also studied dispersion and dissipation errors of the LB scheme and compared the result to various Navier-Stokes solvers. Their results highlighted the low dissipative nature of lattice Boltzmann models compared with other high order schemes.

More recently, Budinski [1] investigated solving the 1-d water hammer equation, with emphasis on models that configure the computational grid independently of the wave speed. He proposed to use LBM method for one-dimensional problems using the D1Q3 model with three discrete velocities. The governing equations are modified using appropriate coordinate transformations to eliminate grid limitations related to the method of characteristics.

This paper addresses the following key issues:

1. Modeling water hammer: In the field of hydraulic engineering and transient flows, LBM is not considered to be suitable for modeling compressible flow, and generally the method is avoided. The method of characteristics (MOC) is preferred for modeling transient flows in 1-d and finite volume method or finite difference method are typically used for 2-d water hammer flows. However, this paper shows that LBM is equally accurate as MOC and, since LBM is computationally a very fast method, it could be used to efficiently model 1-d transient flows. Therefore, in the first part of this paper, classical 1-d water hammer applications (e.g. Ghidaoui [15], Chaudhry [4]) are modeled using LBM and compared with MOC results to evaluate the accuracy and performance of LBM scheme relative to MOC.

2. In the second part of this paper, the 2-d water hammer case is modeled using LBM. Comparison with a 5th order finite volume

(FV) scheme shows that LBM suffers from dissipation and dispersion at sharp discontinuities and when simulating radial oscillations. Notice that the preservation of sharp and continuous wavefronts in water hammer actually requires maintenance of longitudinal waves at high frequency in the numerical scheme. Although a sharper wavefront could be maintained in LBM by mesh refinement, an alternative approach is considered in this paper by investigating the dissipation effects in LBM considering smooth high frequency waves where the longitudinal (plane wave) mode and radial modes propagate separately.

Because radial and longitudinal wave modes may have different dissipation mechanisms, multi-relaxation time (MRT) LBM is used in this study to allow separate treatment of the bulk and shear viscosity terms. In fact, the results show that radial wave dissipation is governed by the bulk viscosity whereas dissipation of longitudinal waves is dictated by shear viscosity. In addition, the MRT scheme has additional free parameters that have no analogous physical interpretation but which do affect the stability of the LBM scheme and also affect accuracy of the boundary conditions [14] solutions. Other variants of the LBM scheme can also be used, such as two relaxation times (TRT) [17], single relaxation time (SRT) [17], or other LBM schemes using different collision operators such as entropic lattice Boltzmann (ELBM) [6] and cumulant lattice Boltzmann (CLBM) [16]. In fact, the ELBM scheme claims that it respects the discrete H theorem while CLBM uses more general equilibrium distributions than those of the MRT scheme. The choice to use MRT LBM in this work is based on its simplicity and popularity. Future work will examine in more depth the performance of other LBM schemes.

2. Lattice Boltzmann scheme for water hammer application

2.1. One-dimensional case

This section describes the lattice Boltzmann scheme for one-dimensional water hammer application. The LB scheme uses three discrete velocities (D1Q3) as shown in Fig. 1. Let $\mathcal{L}$ be a regular lattice parametrized by a space step Δx (see Fig. 1), composed by a set $\mathcal{L}^0 \equiv \{x_j \in (\Delta x \mathbb{Z})\}$ of nodes (or vertices); Δt is the time step of the evolution of LB scheme and $\lambda \equiv \frac{\Delta x}{\Delta t}$ is the numerical celerity. The discrete velocities $v_i, i \in (0, 1, 2)$ are chosen such that $v_i \equiv c_i \frac{\Delta x}{\Delta t} = c_i \lambda$, where the family of vectors $\{c_i\}$ is defined by: $c_0 = 0$, $c_1 = 1$ and $c_2 = -1$. The lattice Boltzmann scheme is given as follows [11]:

$$f_i(x_j, t + \Delta t) = f_i^*(x_j - v_i \Delta t, t), \quad 0 \le i \le 2, \tag{1}$$

where f_i is the discrete probability distribution function corresponding to the ith discrete velocity v_i, t denotes time, x_j is the position of the jth node and the superscript $*$ denotes post-collision quantities. Therefore, during each time increment Δt there are two fundamental steps: advection and collision. The advection step describes the motion of the particles traveling from nodes $x_j - \Delta x$ and $x_j + \Delta x$ with velocities v_1 and v_2, respectively, towards node x_j where the collision step occurs [18]. The collision process is defined by the conservation of moments of order zero (mass) and of order one (momentum) from the pre-collision state to the post-collision state between advected particles and the local particle at node x_j [18]. The three moments $\{m_\ell, \ell \in (0, 1, 2)\}$ are obtained by a linear transformation from the space of discrete probability density functions. These moments are density $m_0 \equiv \rho \equiv f_0 + f_1 + f_2$, momentum $m_1 \equiv q \equiv \rho u \equiv \lambda(f_1 - f_2)$ (where u is the fluid velocity) and energy $m_2 \equiv \epsilon \equiv \frac{\lambda^2}{2}(f_1 + f_2)$. The linear transformation is summarized in matrix form as follows:
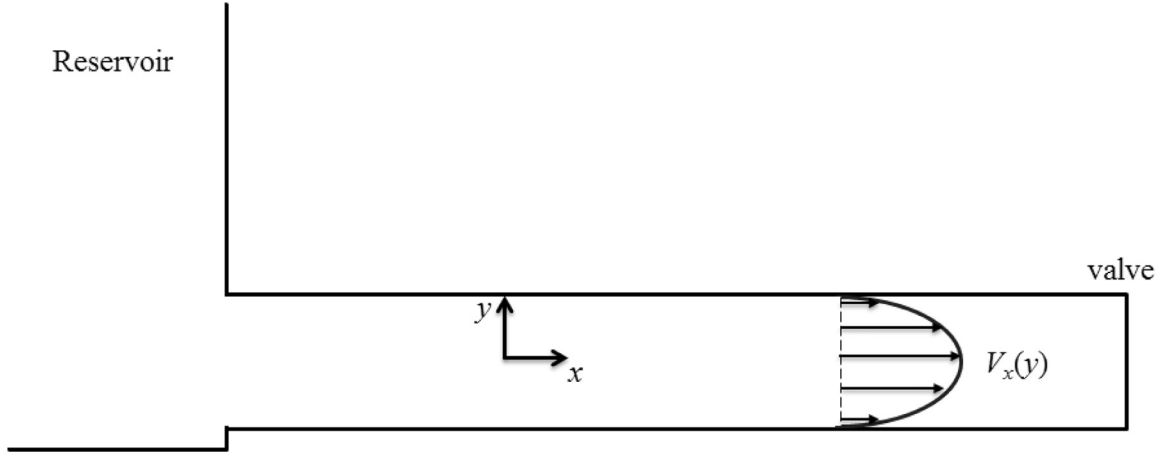
$$(m_0, m_1, m_2)^t = M (f_0, f_1, f_2)^t, \tag{2}$$

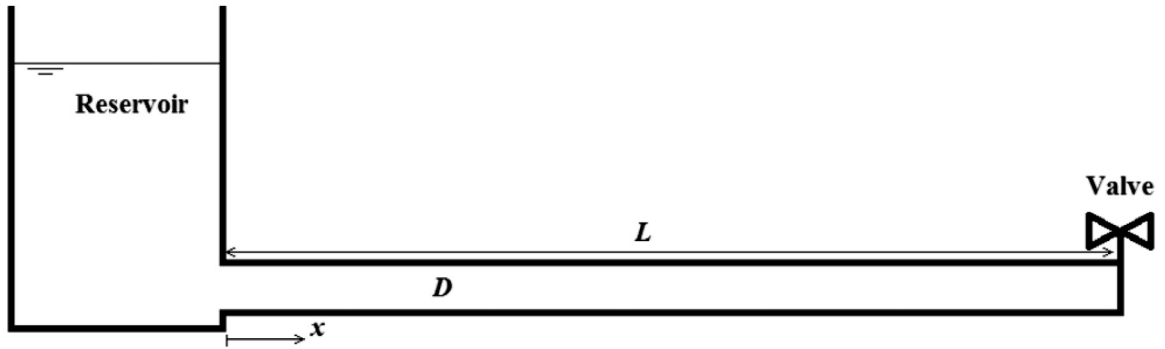**Fig. 3.** Reservoir pipe valve system showing the velocity profile.

Fig. 4. Reservoir pipe valve system.

where

$$M = \begin{pmatrix} 1 & 1 & 1 \\ 0 & \lambda & -\lambda \\ 0 & \frac{\lambda^2}{2} & \frac{\lambda^2}{2} \end{pmatrix}. \tag{3}$$

The non-conserved moment (energy m_2) is assumed to relax towards the equilibrium value (m_2^{eq}) as follows [12]:

$$m_2^* = (1 - s)\, m_2 + s\, m_2^{eq}, \tag{4}$$

where s ($s > 0$) is the relaxation rate and the equilibrium value m_2^{eq} is defined as

$$m_2^{eq} = \frac{1}{2}\left(\alpha \lambda^2 \rho + \rho\, u^2\right). \tag{5}$$

The above expression Eq. (5) is obtained from the second order moment $\int_{\mathbb{R}} f^0 u^2 du$ where f^0 is the Maxwellian distribution function. Consequently, using Taylor expansion at order 2 [12], the following two macroscopic equations are obtained from the advection and collision steps :

$$\begin{cases} \partial_t \rho + \partial_x q = O(\Delta t^2), \\ \partial_t q + c_s^2\, \partial_x \rho + \partial_x(\rho u^2) - \nu_0\, \partial_x^2 q = O(\Delta t^2), \end{cases} \tag{6}$$

where $c_s = \lambda \sqrt{\alpha}$ is the equivalent sound speed and

$$\nu_0 = \lambda^2 \Delta t (1 - \alpha)\left(\frac{1}{s} - \frac{1}{2}\right) \tag{7}$$

is the equivalent kinematic viscosity. The m_2^{eq} moment Eq. (5) determines the macroscopic behavior Eq. (6) of the scheme Eq. (1).

The state equation relating the pressure to the fluid density is

$$\frac{\partial P}{\partial \rho} = c_s^2, \tag{8}$$

where c_s is the wave speed. Eq. (8) is for rigid pipe and in this case c_s is about 1440 m/s when the fluid is water. However, for simplicity in this work, c_s is taken equal to 1000 m/s although Eq. (8) is used.

Note that in this one-dimensional model, there is only one relaxation parameter (s). Therefore, with the linear transformation between the $\{m_\ell\}$ and $\{f_i\}$ spaces, Eq. (2) and the equilibrium distribution in moment space:

$$m_0 = m_0^{eq} = \rho, \quad m_1 = m_1^{eq} = q, \quad m_2^{eq} = \frac{1}{2}\left(\alpha \lambda^2 \rho + \rho u^2\right),$$

the following thermodynamic equilibrium is obtained (in f space):

$$\begin{cases} f_0^{eq} = m_0^{eq} - \frac{2}{\lambda^2} m_2^{eq} = (1 - \alpha)\rho - \frac{\rho u^2}{\lambda^2}, \\ f_1^{eq} = \frac{1}{2\lambda} m_1^{eq} + \frac{1}{\lambda^2} m_2^{eq} = \frac{\rho u}{2\lambda} + \frac{1}{2}\left(\alpha \rho + \frac{\rho u^2}{\lambda^2}\right), \\ f_2^{eq} = -\frac{1}{2\lambda} m_1^{eq} + \frac{1}{\lambda^2} m_2^{eq} = -\frac{\rho u}{2\lambda} + \frac{1}{2}\left(\alpha \rho + \frac{\rho u^2}{\lambda^2}\right). \end{cases} \tag{9}$$

which describes the classical BGK distribution (see [20]).

2.2. Two-dimensional case

In the two-dimensional case, the regular lattice $\mathcal{L}$ becomes as shown in Fig. 2 comprising a set $\mathcal{L}^0 \equiv \{x_{i,j} \in (\Delta x \mathbb{Z}, \Delta y \mathbb{Z})\}$ of nodes (or vertices) with $\Delta x = \Delta y$. Similar to the previous one-dimensional case, the LB scheme in two-dimensions (2-d) is given by:

$$f_i(x_j, t + \Delta t) = f_i^*(x_j - v_i \Delta t, t), \quad 0 \leq i \leq 8, \tag{10}$$
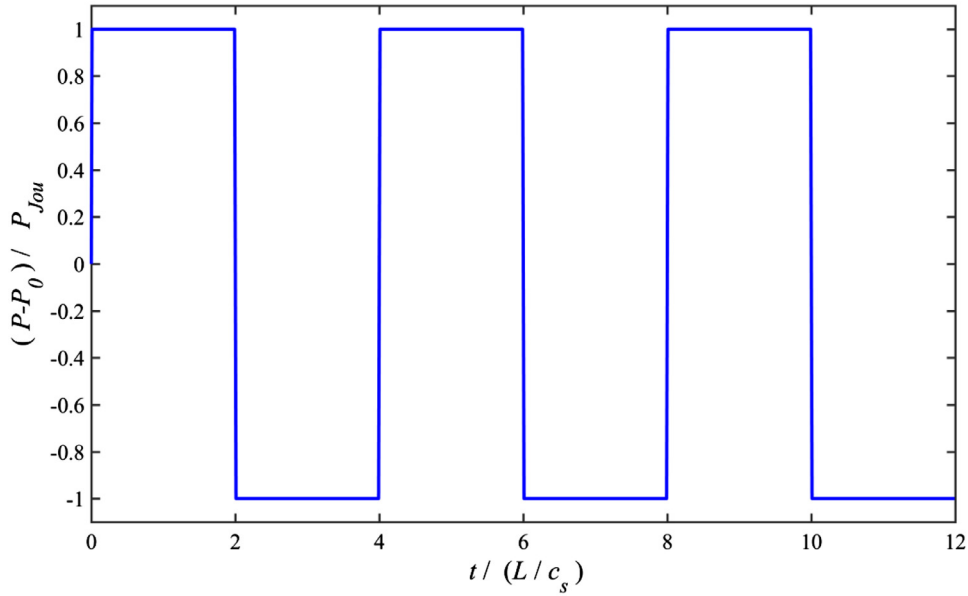
Fig. 5. 1-d LB solutions of the water hammer equation. Dimensionless pressure versus time at the pipe valve where $\alpha = 1$ and $v_0 = 0$.
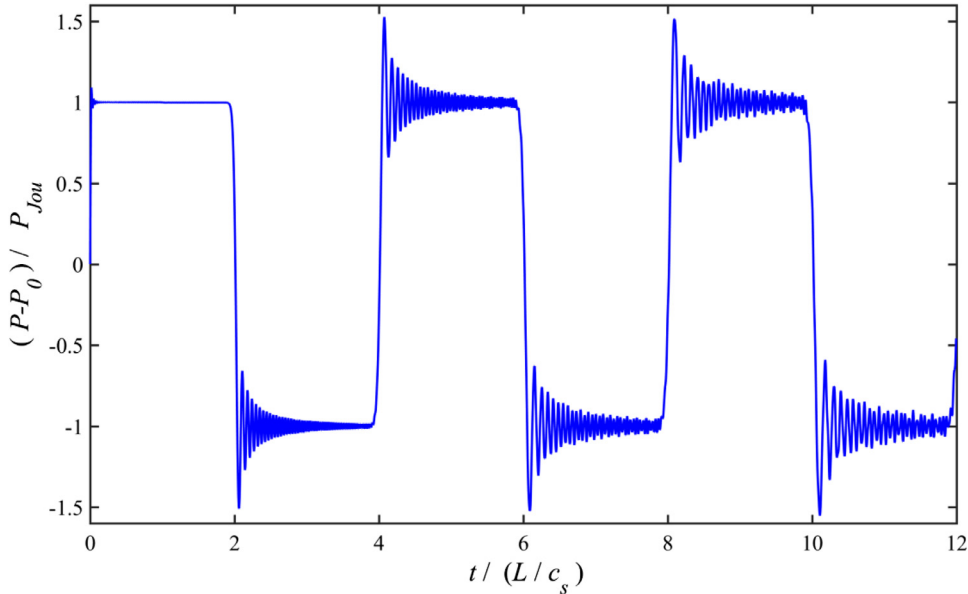

Fig. 6. 1-d LB solutions of the water hammer equation. Dimensionless pressure versus time at the pipe valve where $\alpha = 1/3$ and $v_0 = 10^{-6}$.

which in this case, uses nine discrete velocities $v_i = \lambda c_i$ (D2Q9) (see Fig. 2) where $c_0 = (0, 0)$, $c_1 = (1, 0)$, $c_2 = (0, 1)$, $c_3 = (-1, 0)$, $c_4 = (0, -1)$, $c_5 = (1, 1)$, $c_6 = (-1, 1)$, $c_7 = (-1, -1)$ and $c_8 = (1, -1)$. Again, the scheme is based on the advection and collision steps as described in the 1-d case. However, in the 2-d case the scheme deals with nine moments $\{m_k, k = 0, \ldots, 8\}$. These moments have an explicit physical meaning (see e.g. [20]): $m_0 = \rho$ is the density, $m_1 = j_x$ and $m_2 = j_y$ are x−momentum, y−momentum, m_3 is the energy, m_4 is proportional to energy squared, m_5 and m_6 are x−energy and y−energy fluxes and m_7, m_8 are diagonal and off-diagonal stresses [20]. The same linear transformation Eq. (2) is used to obtain the domain of moments from the domain of distribution functions $\{f_k, k = 0, \ldots, 8\}$ where the matrix M is given in Eq. (A.1). The equivalent Navier–Stokes equations are obtained by conserving three moments namely: $m_0 = \rho$ density, $m_1 = j_x = \rho V_x$ and $m_2 = j_y = \rho V_y$ the x−momentum and y−momentum, respectively. The other non-conserved moments are

assumed to relax towards equilibrium values (m_ℓ^{eq}) obeying the following relaxation equation [18]:

$$m_\ell^* = (1 - s_\ell)\, m_\ell + s_\ell\, m_\ell^{eq}, \quad 3 \le \ell \le 8, \tag{11}$$

where the equilibrium values are given by Eq. (A.2) and where s_ℓ ($0 < s_\ell < 2$, for $\ell \in \{3, 4, \ldots, 8\}$) are relaxation rates, not necessarily equal to a single value as in the so-called BGK scheme [29]. The coefficients α and β are tuning parameters which will be fixed later.

Expanding Eq. (10) using Taylor series, the equivalent macroscopic equations of order two are Eqs. (A.3)–(A.5).

Inserting $j_x = \rho V_x$ and $j_y = \rho V_y$ in the equivalent macroscopic equations (see Eqs. (A.3)–(A.5)), yields:

$$\frac{\partial \rho}{\partial t} + \frac{\partial \rho V_x}{\partial x} + \frac{\partial \rho V_y}{\partial y} = 0, \tag{12}$$
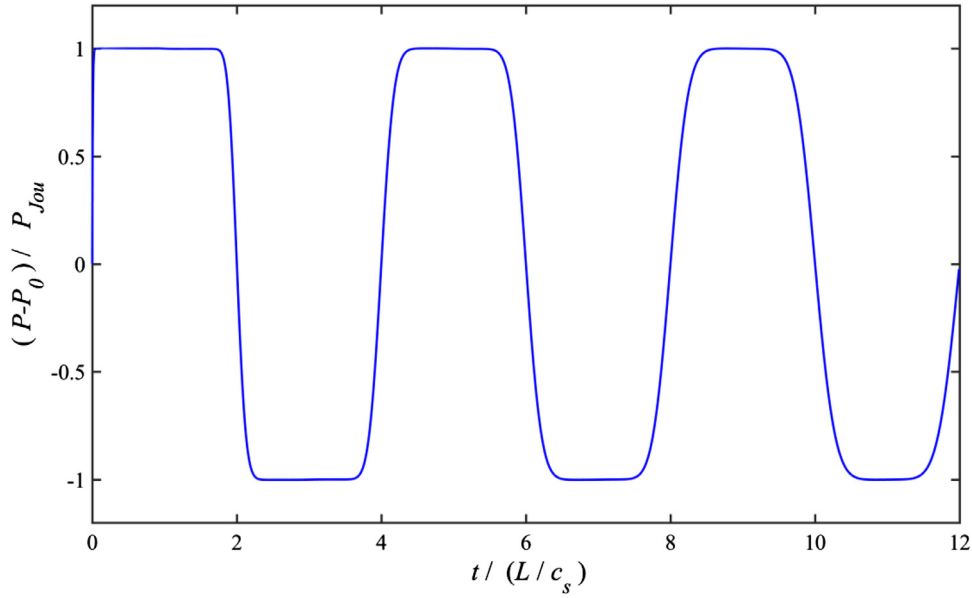
Fig. 7. 1-d LB solutions of the water hammer equation. Dimensionless pressure versus time at the pipe valve where $\alpha = 1/3$ and $s = 1.1$ (i.e. $\nu_0 = 5000$).

$$
\frac{\partial \rho V_x}{\partial t} + \lambda^2 \frac{\alpha + 4}{6} \frac{\partial \rho}{\partial x} + \frac{\partial}{\partial x} \rho V_x^2 + \frac{\partial}{\partial y} \rho V_x V_y
$$
$$
= \frac{\lambda^2}{3} \Delta t \left[\frac{-\alpha}{2} \left(\frac{1}{s_3} - \frac{1}{2} \right) \rho \frac{\partial}{\partial x} \left(\frac{\partial V_x}{\partial x} + \frac{\partial V_y}{\partial y} \right) \right.
$$
$$
\left. + \left(\frac{1}{s_8} - \frac{1}{2} \right) \rho \left(\frac{\partial^2}{\partial x^2} + \frac{\partial^2}{\partial y^2} \right) V_x \right]
$$
$$
+ \left\{ \frac{-\alpha \lambda^2}{6} \Delta t \left(\frac{1}{s_3} - \frac{1}{2} \right) \left(V_x \frac{\partial^2 \rho}{\partial x^2} + 2 \frac{\partial \rho}{\partial x} \frac{\partial V_x}{\partial x} \right. \right.
$$
$$
\left. + V_y \frac{\partial^2 \rho}{\partial x \partial y} + \frac{\partial \rho}{\partial x} \frac{\partial V_y}{\partial y} + \frac{\partial \rho}{\partial y} \frac{\partial V_y}{\partial x} \right)
$$
$$
+ \frac{\lambda^2}{3} \Delta t \left(\frac{1}{s_8} - \frac{1}{2} \right) \left(V_x \frac{\partial^2 \rho}{\partial x^2} + 2 \frac{\partial \rho}{\partial x} \frac{\partial V_x}{\partial x} \right.
$$
$$
\left. \left. + V_x \frac{\partial^2 \rho}{\partial y^2} + 2 \frac{\partial \rho}{\partial y} \frac{\partial V_x}{\partial y} \right) \right\},
\tag{13}
$$

$$
\frac{\partial \rho V_y}{\partial t} + \lambda^2 \frac{\alpha + 4}{6} \frac{\partial \rho}{\partial y} + \frac{\partial}{\partial x} \rho V_x V_y + \frac{\partial}{\partial y} \rho V_y^2
$$
$$
= \frac{\lambda^2}{3} \Delta t \left[\frac{-\alpha}{2} \left(\frac{1}{s_3} - \frac{1}{2} \right) \rho \frac{\partial}{\partial y} \left(\frac{\partial V_x}{\partial x} + \frac{\partial V_y}{\partial y} \right) \right.
$$
$$
\left. + \left(\frac{1}{s_8} - \frac{1}{2} \right) \rho \left(\frac{\partial^2}{\partial x^2} + \frac{\partial^2}{\partial y^2} \right) V_y \right]
$$
$$
+ \left\{ \frac{-\alpha \lambda^2}{6} \Delta t \left(\frac{1}{s_3} - \frac{1}{2} \right) \left(V_y \frac{\partial^2 \rho}{\partial y^2} + 2 \frac{\partial \rho}{\partial y} \frac{\partial V_y}{\partial y} \right. \right.
$$
$$
\left. + V_x \frac{\partial^2 \rho}{\partial x \partial y} + \frac{\partial \rho}{\partial x} \frac{\partial V_x}{\partial y} + \frac{\partial \rho}{\partial y} \frac{\partial V_x}{\partial x} \right)
$$
$$
+ \frac{\lambda^2}{3} \Delta t \left(\frac{1}{s_8} - \frac{1}{2} \right) \left(V_y \frac{\partial^2 \rho}{\partial x^2} + 2 \frac{\partial \rho}{\partial x} \frac{\partial V_y}{\partial x} \right.
$$
$$
\left. \left. + V_y \frac{\partial^2 \rho}{\partial y^2} + 2 \frac{\partial \rho}{\partial y} \frac{\partial V_y}{\partial y} \right) \right\}
\tag{14}
$$

where V_x and V_y are the flow velocities along the x and y directions, respectively. Notice that the above equivalent macroscopic equations contain additional terms (shown between curly brackets in Eqs. (13) and (14)) with respect to the Navier–Stokes equations. It can be shown that these additional terms are negligible with respect to the viscous terms.

2.3. 2-d classical water hammer test case

This section considers the case of viscous-laminar flow as shown in Fig. 3. Notice that in this case y represents the radial coordinate and V_y is the radial velocity. The initial conditions are constant initial velocity and pressure along the pipe given as follows:

$$
\begin{cases}
V_x(y) = 2V_x^0 \left(1 - \dfrac{y^2}{R^2} \right), & 0 \le y \le R, \\[2mm]
P(x) = p_0 - \dfrac{32 \, \rho_0 V_x^0 \, \nu}{D^2} x, & 0 \le x \le L.
\end{cases}
\tag{15}
$$

where $\nu = $ kinematic viscosity in water ($\nu = 10^{-6}$ m^2/s); $D = 2R = $ pipe diameter ($D = 0.4$) m with R the pipe radius; $V_x^0 = $ constant mean velocity; $\rho_0 = $ initial density ($\rho_0 = 1000$ kg/m^3); $p_0 = $ constant initial gauge pressure in the pipe. It is important to note that, in a cylindrical coordinate system, additional geometrical terms are added to the 2-d Navier–Stokes equations which are given below:

$$
\frac{\partial \rho}{\partial t} + \frac{\partial \rho V_y}{\partial y} + \frac{\partial \rho V_x}{\partial x} = \underbrace{-\frac{\rho V_y}{y}}_{\text{Term due to radial coordinates system}}
\tag{16}
$$

$$
\frac{\partial \rho V_y}{\partial t} + c_s^2 \frac{\partial \rho}{\partial y} + \frac{\partial}{\partial r} \rho V_y^2 + \frac{\partial}{\partial x} \rho V_y V_x
$$
$$
= \left[(\mu + \lambda) \frac{\partial}{\partial y} \left(\frac{\partial V_y}{\partial y} + \frac{\partial V_x}{\partial x} \right) + \mu \Delta V_y \right]
$$
$$
+ \underbrace{\frac{2\mu + \lambda}{y} \left(\frac{\partial V_y}{\partial y} - \frac{V_y}{y} \right) - \frac{\rho}{y} V_y^2}_{\text{Terms due to radial coordinates system}},
\tag{17}
$$

Fig. 8. 2-d LB solutions of the water hammer equation. Dimensionless pressure versus time at the pipe valve at the pipe centerline where $s_3 = 1.75$, $s_8 = 1.4$ (*i.e.* $v_0 = 0.49$) and $N_y = 100$.
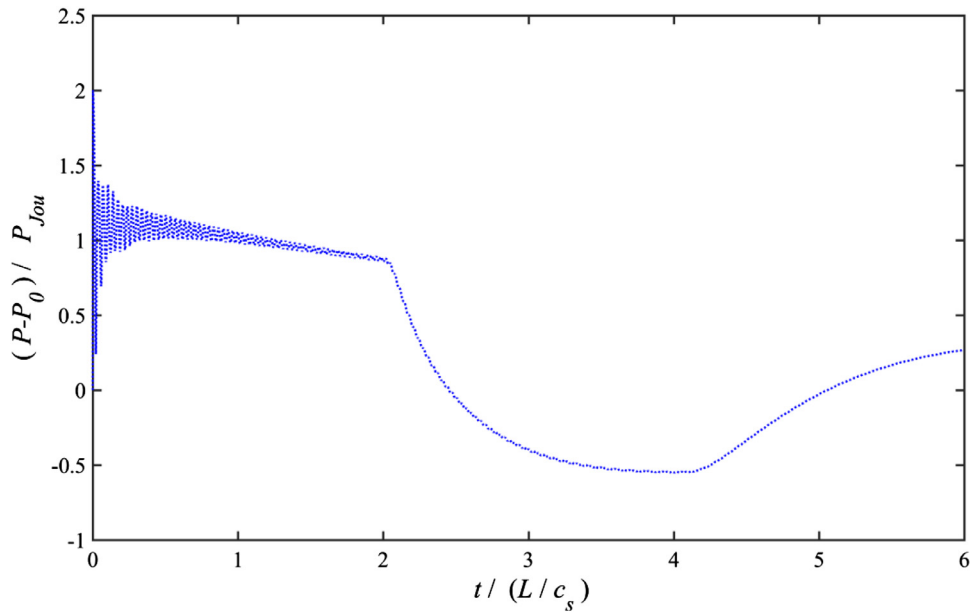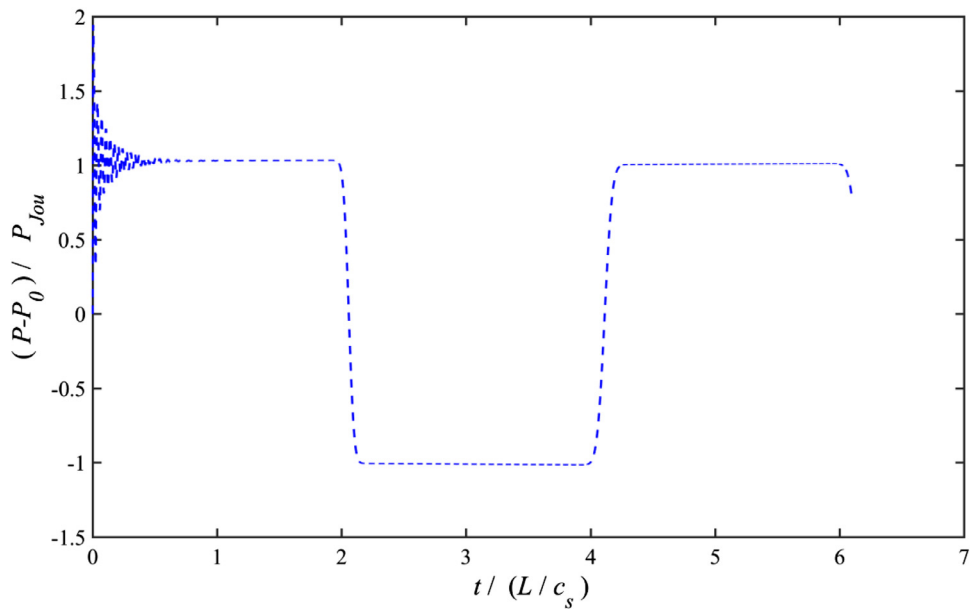

Fig. 9. 2-d LB solutions of the water hammer equation. Dimensionless pressure versus time at the pipe valve at the pipe centerline where $s_3 = 1.1$, $s_8 = 1.99965$ (*i.e.* $v_0 = 10^{-3}$) and $N_y = 20$.

$$
\frac{\partial \rho V_x}{\partial t} + c_s^2 \frac{\partial \rho}{\partial x} + \frac{\partial}{\partial y} \rho V_y V_x + \frac{\partial}{\partial x} \rho V_x^2
$$

$$
= \left[(\mu + \lambda) \frac{\partial}{\partial x} \left(\frac{\partial V_y}{\partial y} + \frac{\partial V_x}{\partial x} \right) + \mu \Delta V_x \right]
$$

$$
+ \underbrace{\frac{\mu + \lambda}{y} \frac{\partial V_x}{\partial x} + \frac{\mu}{y} \frac{\partial V_x}{\partial y} - \frac{\rho}{y} V_y V_x}_{\text{Terms due to radial coordinates system}} , \tag{18}
$$

where V_x is the x–velocity and V_y is the y–velocity. The D2Q9 scheme introduced in the above section is used to solve Eqs. (16)–(18). Note that by using LBM, the equivalent equations are slightly different from the continuous problem. The additional geometrical terms are added to the LBM scheme using operator splitting of order 2.

2.4. Boundary conditions

The boundary conditions are essentially to impose a non slip condition on the wall or to impose a given pressure/velocity in upstream/downstream boundaries. To perform these boundary conditions, anti-bounce back [17] scheme and bounce back [14] scheme are used to impose a given pressure and a given velocity, respec-
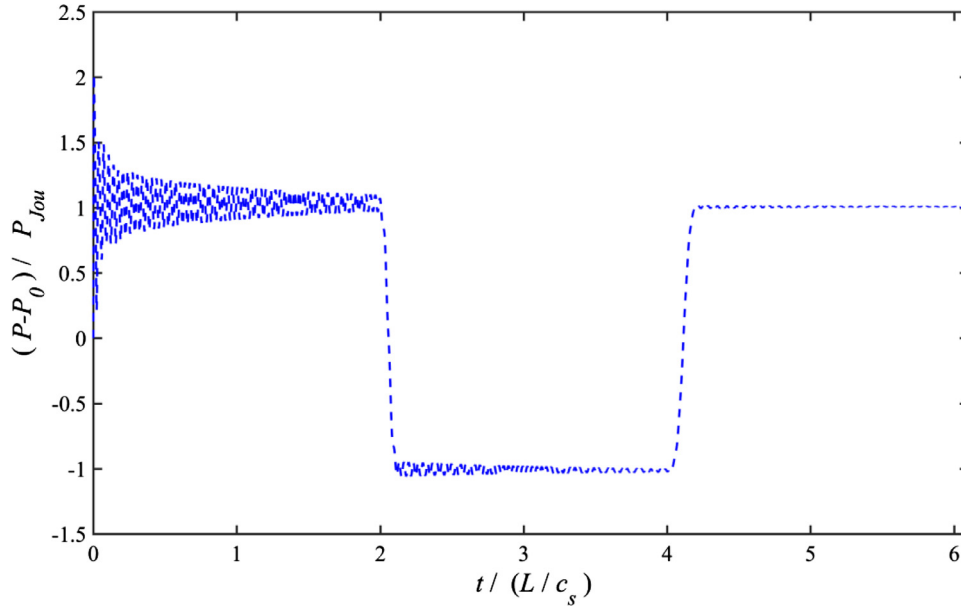
Fig. 10. 2-d LB solutions of the water hammer equation. Dimensionless pressure versus time at the pipe valve at the pipe centerline where $s_3 = 1.45$, $s_8 = 1.99965$ (*i.e.* $v_0 = 10^{-3}$) and $N_y = 20$.
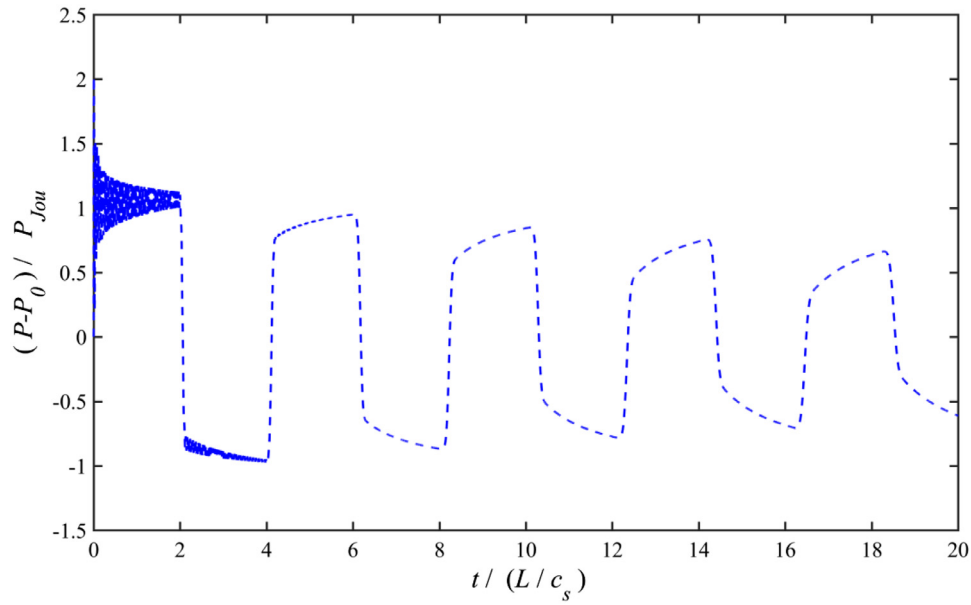

Fig. 11. 2-d LB solutions of the water hammer equation. Dimensionless pressure versus time at the pipe valve at the pipe centerline where $s_3 = 1.45$, $s_8 = 1.9965$ (*i.e.* $v_0 = 10^{-2}$) and $N_y = 20$.

tively. The detail of bounce back and anti-bounce back schemes are given in next section.

3. Numerical results and discussion

3.1. 1-d classical water hammer test case

The 1-d water hammer test case consists of sudden closure of a downstream valve in a reservoir-pipe-valve (RPV) system with an initial non-zero flow [33] (see Fig. 4). The boundary conditions require pressure to be constant at the upstream (reservoir) for all time, and the velocity to be zero at the downstream ($V_x = 0$). These boundary conditions are imposed as follows:

• Upstream boundary $P(x = 0) = p_0$: To impose pressure on the inlet, anti-bounce back [3] boundary condition is performed:

$$f_1(x_1) = -f_2^*(x_1) + \alpha \rho_0, \qquad (19)$$

where $\rho_0 = \frac{p_0}{c_s^2}$ is given by the boundary condition and x_1 is the first fluid node.

Remark. The above anti-bounce back condition is obtained by taking the distribution f_1 and f_2 at equilibrium (see Eq. (9)) at the boundary.

• Downstream boundary $V_x(x = L) = 0$: To model $V_x = u_0 = 0$ on the outlet bounce back boundary condition is performed:
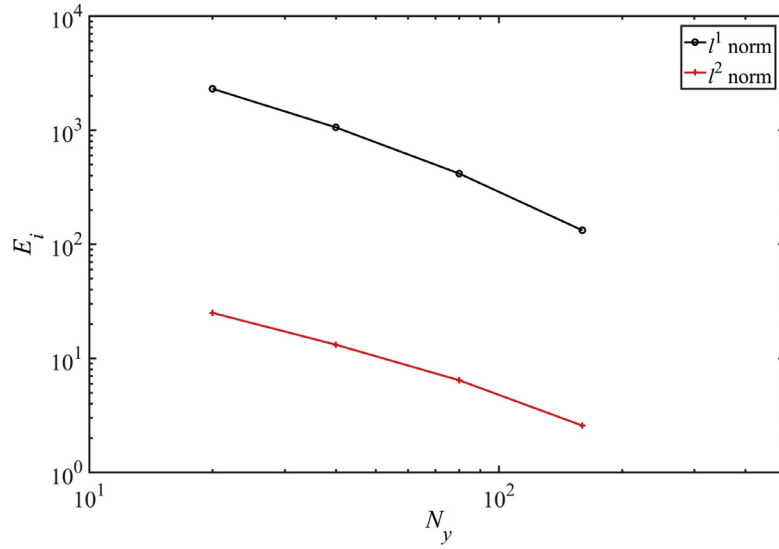
$$f_2(x_N) = f_1^*(x_N) + \frac{\rho u_0}{\lambda}, \qquad (20)$$
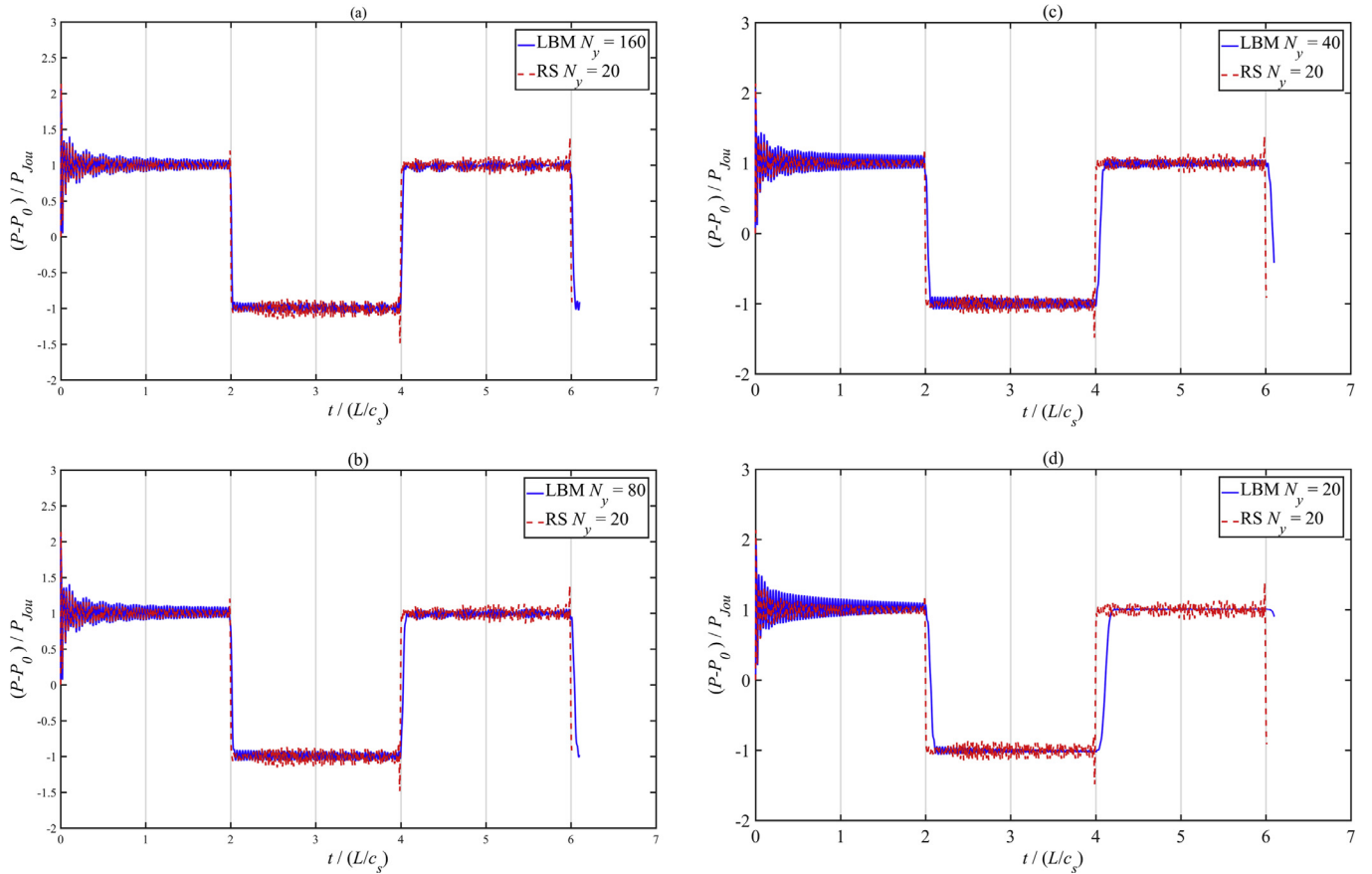
Fig. 12. Convergence test.

Fig. 13. Dimensionless pressure versus time at the valve and at the pipe centerline using Riemann Solver 3rd/5th order (RS) with $N_y = 20$ and using LBM $s_3 = 1.45$, $s_8 = 1.99965$ (*i.e.* $\nu_0 = 10^{-3}$) and different mesh sizes : (a) $N_y = 160$, (b) $N_y = 80$, (c) $N_y = 40$ and (d) $N_y = 20$.

where $u_0 = 0$ is given by boundary condition and x_N is the last fluid node.

Remark. To keep the stability of the scheme, the parameter α must be in the interval [0,1] because the term $(1 - \alpha)$ in Eq. (6) must be positive.

For all cases, the length of the pipe is $L = 1000$ m and the mesh size is $N_x = 101$. Thus, the space step is $\Delta x = L/N_x$ and the numer-

ical wave speed is $c_s = \frac{\Delta x}{\Delta t}\sqrt{\alpha}$. The time step and relaxation parameter are given by: $\Delta t = \sqrt{\alpha}\frac{\Delta x}{c_s}$ and $s = \left(\frac{\nu_0}{\lambda \Delta x(1 - \alpha)} + \frac{1}{2}\right)^{-1}$, respectively. Only the parameter α remains unfixed. In fact this parameter represents the Courant–Friedrichs–Lewy (CFL) number, which is defined by:

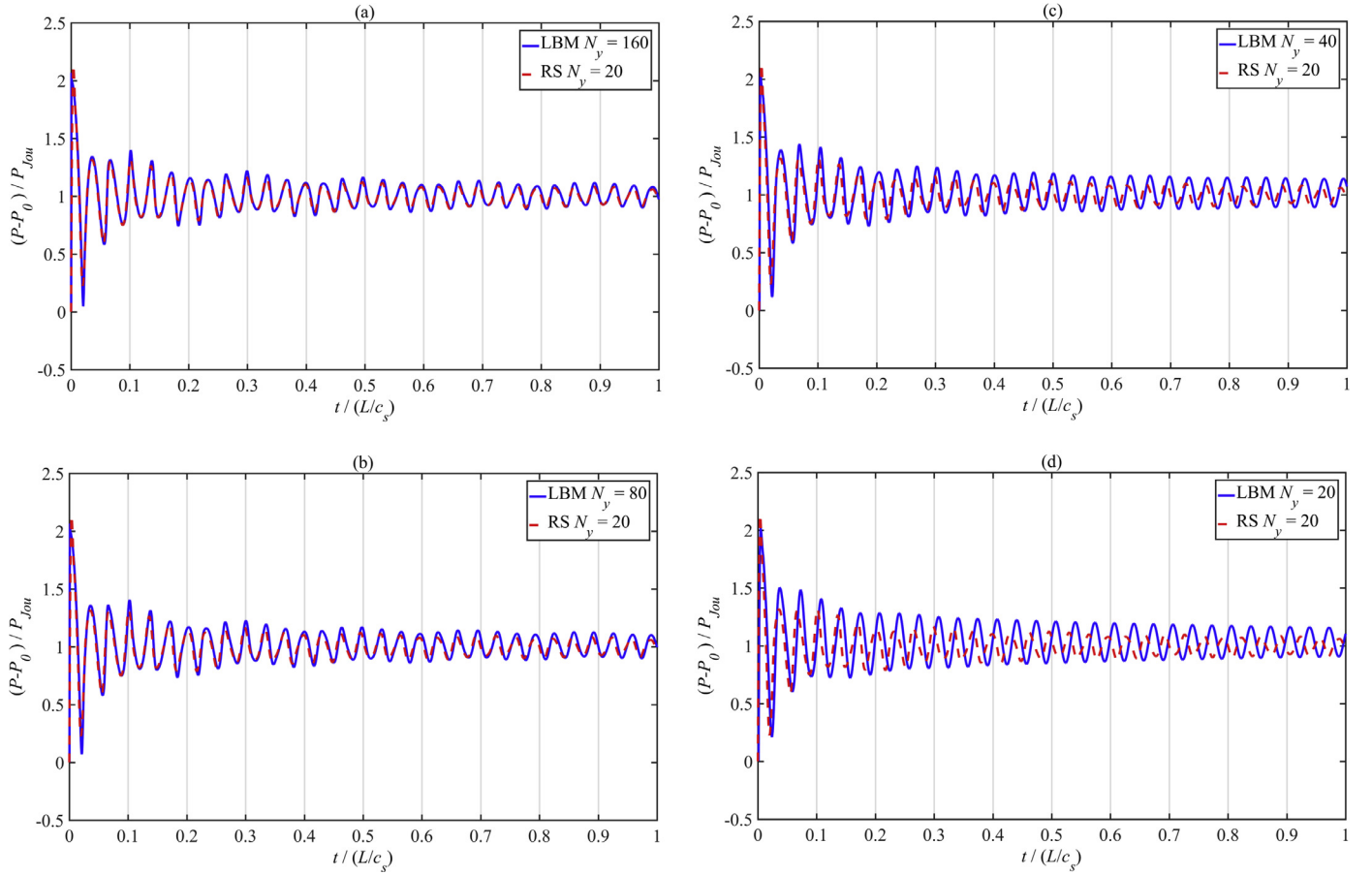$$\sqrt{\alpha} = c_s \frac{\Delta t}{\Delta x} . \tag{21}$$

Fig. 14. Zoomed version of Fig. 13 in the time interval $[0, L/c_s]$.

Note that for the case $\alpha = 1$ the equivalent kinematic viscosity (ν_0) (see Eq. (7)) becomes zero, and therefore the LB macroscopic equations (see Eq. (6)) are equivalent to the inviscid 1-d water hammer equations [15].

Three test cases are considered for different values of α and s :

1. $\alpha = 1$, in this case the numerical viscosity (ν_0) is zero for any s value. Therefore the flow is inviscid.
2. $\alpha = 1/3$ and s is such that $\nu_0 = 10^{-6}$ m^2/s which is equal to the actual kinematic viscosity value for water.
3. $\alpha = 1/3$ and $s = 1.1$.

Figs. 5–7 give dimensionless pressure variations with time measured at the valve. The pressure is normalized by the Joukowsky pressure ($P_{Jou} = \rho_0 V_x^0 c_s$) for cases 1, 2 and 3, respectively. Case 1 ($\alpha = 1$) is depicted in Fig. 5, which shows that LBM gives the exact solution of water hammer pressure variation for a RPV system with inviscid flow. The exact solution is known from the method of characteristics (MOC) solution and can be found in [33]. This result is interesting because LBM usually solves viscous flows.

In addition the LB scheme (in the case $\alpha = 1$ and $s = 1$) is equivalent to the following finite difference scheme:

$$\begin{cases} \rho_j^{n+1} = \frac{1}{2}\left(\rho_{j+1}^n + \rho_{j-1}^n\right) + \frac{1}{2\lambda}\left(q_{j+1}^n - q_{j-1}^n\right), \\ q_j^{n+1} = \frac{1}{2}\left(q_{j+1}^n + q_{j-1}^n\right) - \frac{\lambda}{2}\left(\rho_{j+1}^n - \rho_{j-1}^n\right), \end{cases} \quad (22)$$

which is the solution of the density and momentum obtained by the method of characteristics; where n denotes the nth time step and j is the position of the jth node.

In case 2, viscous flow is considered, and viscosity is chosen to be equal to the actual kinematic viscosity value for water ($\nu_0 = 10^{-6}$ m^2/s). In this case, Fig. 6 shows that the scheme

reaches its limit of stability. This is because the parameter s governs the viscous term in Eq. (6) and becomes almost 2 ($s = 1.999999999650126$) whereas s must be strictly less than 2 for the scheme to remain stable.

In case 3, typical values of α and s are taken ($\alpha = 1/3$ and $s = 1.1$). For these values, the numerical kinematic viscosity is about $\nu_0 = 5000$ m^2/s. However, Fig. 7 shows that the signal is slightly damped. Therefore, the numerical viscosity does accurately represent the actual flow viscosity. This may be due to higher order terms neglected when deriving the macroscopic equations (see Eq. (6)).

3.2. 2-d classical water hammer test case

This section considers the problem described in the section 1.3, and solves the macroscopic equations Eqs. (12)–(14) using LB. Consider the domain $\Omega = [0, L] \times [0, H]$ and the regular mesh (lattice) $\mathcal{L}^0 = \{x_{i,j} \in \Delta x \mathbb{Z} \times \Delta y \mathbb{Z}, 1 \leq i \leq N_x, 1 \leq j \leq N_y\}$ parametrized by the space step $\Delta x = \Delta y$. The boundary conditions are like those in the previous section with the additional constraints of zero radial velocity and no slip condition at the pipe walls. In more detail, the boundary conditions are as follows:

- Upstream boundary ($P(x = 0) = p_0$): To impose p_0, anti-bounce back is performed as follows:

$$\begin{cases} f_1(x_{(1,j)}) = -f_3(x_{(0,j)}) + \frac{4-\alpha-2\beta}{18}\frac{p_0}{c_s^2}, \\ f_5(x_{(1,j)}) = -f_7(x_{(0,j-1)}) + \frac{4+2\alpha+\beta}{18}\frac{p_0}{c_s^2}, \\ f_8(x_{(1,j)}) = -f_6(x_{(0,j+1)}) + \frac{4+2\alpha+\beta}{18}\frac{p_0}{c_s^2} \end{cases} \quad (23)$$

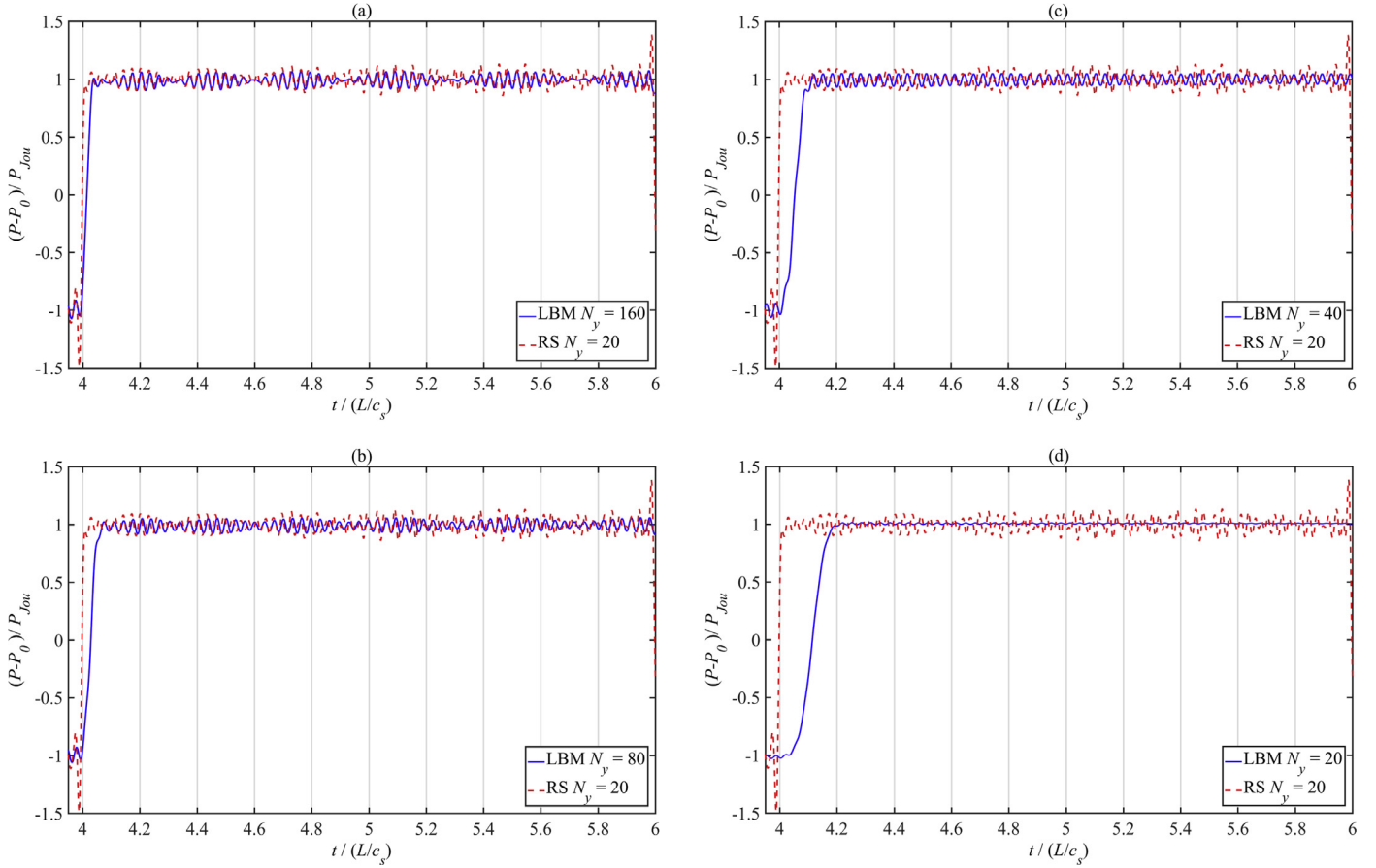where p_0 is given by the boundary condition and $1 \leq j \leq N_y$.

Fig. 15. Zoomed version of Fig. 13 in the time interval $[4L/c_s, 6L/c_s]$.

- Downstream boundary $(V_x(x = L) = 0)$: To impose $V_x = 0$, bounce back is performed as follows:

$$\begin{cases} f_3(x_{(N_x,j)}) = f_1(x_{(N_x+1,j)}), \\ f_6(x_{(N_x,j)}) = f_8(x_{(N_x+1,j+1)}), \\ f_7(x_{(N_x,j)}) = f_5(x_{(N_x+1,j-1)}) \end{cases} \quad (24)$$

where $1 \leq j \leq N_y$.

- Pipe wall boundary $(V_y(y = R) = 0)$: To impose $V_y = 0$, bounce back is performed as follow: Bounce back for $x_{i,1}$ and x_{i,N_y} where $1 \leq i \leq N_x$:

$$\begin{cases} f_4(x_{(i,1)}) = f_2(x_{(i,0)}), \\ f_5(x_{(i,1)}) = f_7(x_{(i-1,0)}), \\ f_6(x_{(i,1)}) = f_8(x_{(i+1,0)}). \end{cases} \quad (25)$$

$$\begin{cases} f_4(x_{(i,N_y)}) = f_2(x_{(i,N_y+1)}), \\ f_7(x_{(i,N_y)}) = f_5(x_{(i-1,N_y+1)}), \\ f_8(x_{(i,N_y)}) = f_6(x_{(i+1,N_y+1)}). \end{cases} \quad (26)$$

The following length scales $L = 1000$ m, $D = 0.4$ m and mesh size $N_y = 20, 160$ and 500, $N_x = \frac{N_y L}{D}$ are considered. The CFL number is given by $C_0 = c_s \frac{\Delta t}{\Delta x} = \frac{c_s}{\lambda}$, where $c_s = \lambda \sqrt{\frac{\alpha+4}{6}} = 1000$ m/s is the wave speed. Therefore the CFL number is $C_0 = \sqrt{\frac{\alpha+4}{6}}$. Thus, the LB parameters are fixed as follows: $\alpha = 6C_0^2 - 4$, $\Delta t = \frac{\Delta x}{c_s} C_0$, $\alpha = -2$, and $\beta = 1$. The time step Δt and space step Δx are fixed to have wave speed $c_s = 1000$ m/s. The other LB relaxation (stability) parameters are fixed by identification between equations Eqs. (13), (14) and Eqs. (17), (18) as follows:

$$\mu_0 = \frac{\lambda^2}{3} \Delta t \left(\frac{1}{s_8} - \frac{1}{2}\right) \rho = \nu_0 \times \rho \quad \Rightarrow \quad s_8 = \frac{1}{\frac{3\nu_0}{\lambda \Delta x} + \frac{1}{2}}, \quad (27)$$

Table 1
Validation of the order of accuracy of the scheme using mesh refinement; the pressure data considered is taken up to $0.95L/c_s$ seconds in time which excludes any pressure jump where $r_m = \frac{\log(E_m/E_{20})}{\log(m/20)}$.

m	ℓ_1	ℓ_2
40	1.1272	0.9280
80	1.2350	0.9810
160	1.3748	1.0947

$$\frac{\mu_0}{3} = \frac{-\alpha\lambda^2}{6} \Delta t \left(\frac{1}{s_3} - \frac{1}{2}\right) \rho \quad \Rightarrow \quad s_3 = \frac{1}{\frac{1}{2} - \frac{2}{3\alpha}\left(\frac{1}{s_8} - \frac{1}{2}\right)}. \quad (28)$$

Eq. (27) satisfies the kinematic viscosity, and Eq. (28) satisfies Stokes relation. For water hammer problem, where $\nu_0 = 10^{-6} m^2/s$, the stability parameters are $s_3 = 1.99999953$ and $s_8 = 1.99999986$. In this case the LB scheme is unstable because s_3 and s_8 approach the limit of stability ($s_3 < 2$, $s_8 < 2$). In what follows, different tests are conducted to find the appropriate relaxation (stability) parameters for the 2-d water hammer application. Figs. 8–11 give the dimensionless pressure variation with time measured at the valve and at the pipe centerline where the pressure is normalized by the Joukowsky pressure ($P_{Jou} = \rho_0 V_x^0 c_s$) for the different cases. Fig. 8 shows the case for the maximum s_8 value to give a stable scheme while the Stokes relation Eq. (28) is maintained. In this case, the scheme is extremely dissipative, and maintaining the Stokes relation is no longer possible. Fig. 9 depicts the case
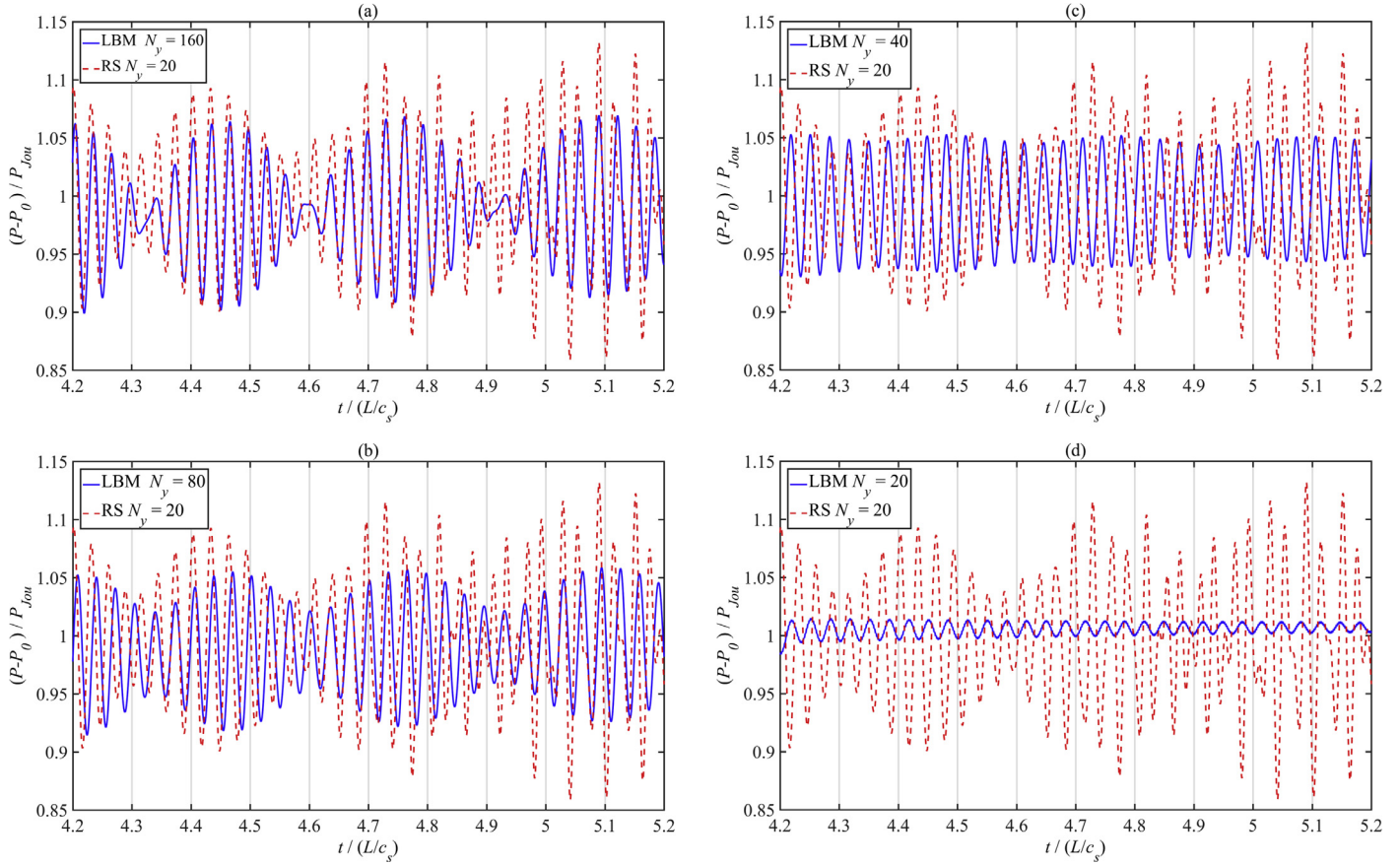
Fig. 16. Zoomed version of Fig. 13 in the time interval $[4.2L/c_s, 5.2L/c_s]$.

Table 2
Validation of the order of accuracy of the scheme using mesh refinement; the pressure data considered is taken up to $6L/c_s$ seconds in time which includes the pressure jumps where $r_m = \frac{\log(E_m/E_{20})}{\log(m/20)}$.

m	ℓ_1	ℓ_2
40	0.8331	0.7228
80	1.0914	0.8368
160	1.2740	1.0034

where $s_8 = 1.99965$ which is chosen such that $\nu_0 = 10^{-3}\,m^2/s$ and s_3 is given a typical value of 1.1. In this case the signal becomes much less dissipative and gives satisfactory results. Note that the oscillations observed in Figs. 8 and 9 are physical, and are due to radial waves (see [22–24]). These radial waves are excited by the idealized (instantaneous) valve closure and propagate along the pipe. However, Fig. 9 shows that these waves are dissipated quickly. Fig. 10 gives the case where s_8 is kept the same but s_3 is increased to its maximum value ($s_3 = 1.45$) while maintaining a stable scheme. In this case, Fig. 10 shows that the radial waves undergo less dissipation while the axial wave dissipation is unchanged. Fig. 11 depicts the case where s_3 is kept to its maximum value 1.45 while s_8 is reduced to $s_8 = 1.9965$ ($\nu_0 = 10^{-2}\,m^2/s$). In this case, Fig. 11 shows that radial wave dissipation remains unchanged while the axial waves become more dissipated than in the previous two cases. This shows that s_3, which relates to the bulk viscosity, governs the dissipation mechanism of radial waves; whereas s_8 governs the dissipation mechanism of axial waves. The values of $s_3 = 1.45$ and $s_8 = 1.99965$ are used for the rest of this paper.

Before continuing further discussion and comparison of the LB scheme with other numerical approaches, it is incumbent to conduct a convergence test using mesh refinement with the fixed relaxation parameters (s_3, s_8). In fact, this is important because s_8 depends on the mesh size (see Eq. (27)). The next subsection gives details of the convergence test and the order of accuracy using mesh refinement with the fixed s_3 and s_8 parameters. The convergence is discussed by comparison with a high order finite volume numerical scheme based on Riemann solver [22,25].

3.3. Order of accuracy and convergence of the scheme using grid refinement

Although the order of accuracy of classical D2Q9 [20] is known to be of order 2 in momentum and of order 1 in pressure (density), this section provides a validation of such order through convergence test. Unfortunately, to the authors' knowledge, there is no available analytical solution for the multi-dimensional water-hammer case. Therefore, the validation of the order of accuracy is conducted by mesh refinement taking a "converged" solution as reference (assumed "exact"). The reference solution is considered for the cases where the mesh is refined to $N_y = 320$ and $N_x = 800,000$. This reference solution is chosen because the error in this case becomes very small (at order 10^{-7}) and the convergence slope remains consistent with the expected order of accuracy. Therefore, the computational mesh is refined where N_y is increased from 20 to 320 and N_x is increased from 50,000 to 800,000, respectively (maintaining $\Delta x = \Delta y$). The ℓ^1 and ℓ^2 norms are used to obtain the following errors $E_m^1 = \| p_m - p_{ref} \|_1$ and $E_m^2 = \| p_m - p_{ref} \|_2$, where $m = \{20, 40, 80, 160\}$ is the mesh size, p_m is the pressure solution, and p_{ref} is a reference (assumed exact) solution which is for the case where $N_y = 320$ and $N_x = 800,000$.
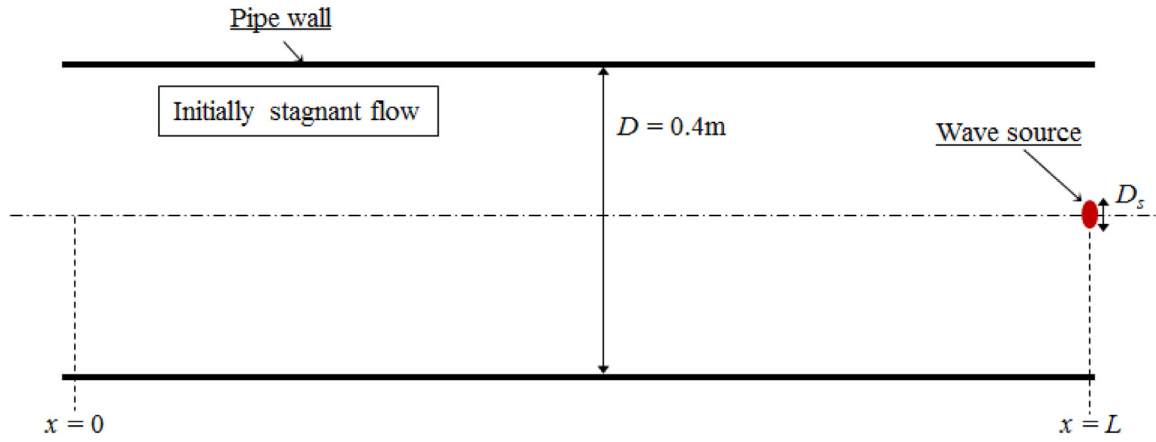
Fig. 17. Sketch of unbounded pipe system.
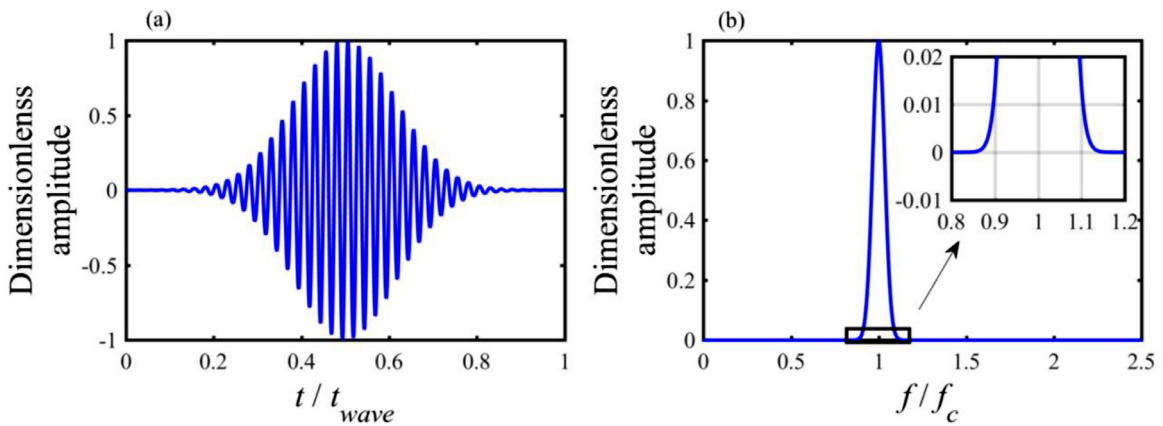

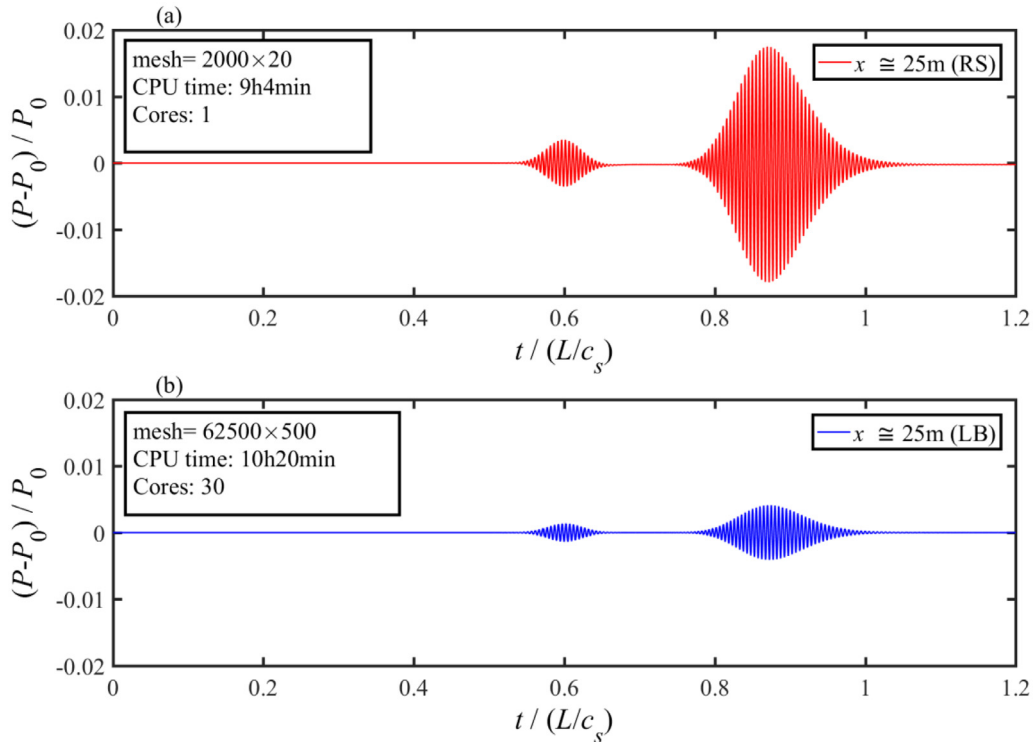**Fig. 18.** Probing wave from ($\widetilde{\beta} = 40\pi$). (a) time domain; (b) frequency domain.

Fig. 19. Dimensionless pressure variation with time at the pipe centerline ($x = 25\,m, y = 0$) where $D_s = 0.2D$. (a) obtained using FVRS scheme. (b) obtained using LBM with $s_3 = 1.45$, $s_8 = 1.99965$.

Fig. 12 gives the errors in logarithmic scale and shows that the slopes of error are 1.2457 of ℓ^1 norm and 1.0012 for ℓ^2 norm which is consistent with the expected order of accuracy of the used LB scheme.

In classical water hammer application, the transient wave is generated by a sudden closure. The pressure rise due to this sudden closure is represented by a vertical line (pressure jump). Such jump can only be (at most) at first order of accuracy even if the scheme is at much higher order. Therefore, for classical water hammer test case, the convergence validation through mesh refinement is done i) using data that excludes the pressure jump (therefore testing the order of the scheme as shown in Table 1 and Fig. 12); ii) using data that includes the pressure jump to see how the scheme catches such jump at order 1 (as shown in Table 2). For example, if a high order FV scheme is used, then a slope limiter must be adopted to reduce the scheme order to 1 at the pressure jump (or hydraulic jump).

The 2-d LB scheme is compared with a 2-d 5th order finite volume numerical scheme based on an approximate Riemann solver (FVRS) [22,25]. The results are shown graphically in Fig. 13. In fact, Fig. 13(a)–(d) show a comparison between the FVRS with N_y fixed at 20 and the LB scheme with $N_y = 160$, $N_y = 80$, $N_y = 40$ and $N_y = 20$, respectively. For clarity, different zoomed areas of these figures at different time intervals are shown. Fig. 14 gives pressure variation up to L/c_s seconds and shows that the LB schemes converges as the mesh is refined. This is mainly because the numerical viscosity of the LB scheme reduces as the mesh becomes refined (see Eq. (27)). The results of radial wave variations in Fig. 14 (a) become identical between both schemes with the refined mesh. Fig. 15 shows the radial wave variation in the time interval $[4.2\,L/c_s, 5.2\,L/c_s]$ seconds. Again, convergence of the LB scheme is observed in the numerical test results with overall good agreement between the two schemes when $N_y = 160$ for the LB scheme (Fig. 15 (a)). However, Fig. 15 (a) shows that besides the slight difference in amplitude between results from the two schemes, the result from the LB scheme is also slightly shifted to the right. This is a dispersion effect. In fact, Fig. 16 shows clearly that the LB scheme suffers from a dispersion effect especially at low mesh size, where the jump location is shifted from its original location ($t = 4\,L/c_s$). Therefore, if the LB scheme is used to model high modes (radial and azimuthal waves modes), which are dispersive in nature, care should be taken to account for the dispersion effect. In this case, a very fine mesh needs to be used to ensure accuracy in modeling the behaviour of dispersive high frequency wave. The next section discusses a particular test case in which dispersive waves of the first high radial mode (M1) are excited and propagate along an infinite pipe system.

3.4. Discussion on the performance of 2nd order LB scheme when modeling dispersive high frequency waves

In this section, a specific numerical test case is designed. This test considers the pipe system shown in Fig. 17 with the following initial conditions:

$$\begin{cases} \rho = \rho_0 = 1000\,\text{kg/m}^3, \\ P = p_0 = \rho_0\,g H_0 = 1000 \times 9.81 \times 10 = 9.81 \times 10^4\,\text{Pa}, \\ V_y = 0,\ V_x = 0, \\ D = 0.4\,m,\ L = 100\,\text{m}, \\ c_s = 1000\,\text{m/s}. \end{cases} \quad (29)$$

The pipe is assumed infinite, and the downstream boundary is located sufficiently far away so that no reflections will interfere with the measured signals. The tests utilize a source located at the upstream boundary ($x = 0$). An acoustic wave is generated from the source and only the right-going wave is considered. The generated waveform at the source is shown in Fig. 18. This form is chosen because it is smooth and allows the modeler to select the desired frequency bandwidth (FBW). Its mathematical form is:

$$\begin{cases} P_f(t) = P_s \exp\left[-4\dfrac{w_c}{\tilde{\beta}^2}\log(10)\left(t - \dfrac{\tilde{\beta}}{w_c}\right)^2\right] \sin\left[w_c(t - \dfrac{\tilde{\beta}}{w_c})\right] \\ \text{where}\ 0 \leq t \leq t_{wave} = \dfrac{\tilde{\beta}}{w_c}, \end{cases} \quad (30)$$

where $w_c = 2\pi\,f_c$ is the angular central frequency (in rad/s) with f_c being the central frequency (in Hz); P_f is the pressure at the source; $P_s = 0.1\,p_0$ is the maximum pressure at the source with p_0 being the initial pressure in the pipe; t_{wave} is the duration of the wave generated at the source; and $\tilde{\beta}$ is a coefficient that controls the FBW. In this work $\tilde{\beta} = 80\,\pi$. The source is considered circular in shape with a given diameter D_s and is located at the pipe centerline. Initially at time $t = 0\,s$, the fluid is at rest. The boundary conditions at the source (the inlet) are

$$\begin{cases} P(r) = \begin{cases} p_0 + P_f & \text{for}\ \ 0 < r < \dfrac{D_s}{2}, \\ p_0 & \text{otherwise.} \end{cases} \\ V_y = 0, \\ \dfrac{\partial V_x}{\partial x} = 0. \end{cases} \quad (31)$$

Pipe wall boundary conditions are similar to the previous 2-d WH test. Because of the dispersive effect of the LB scheme, the LB mesh is refined so that $N_y \times N_x = 500 \times 62500$. This mesh refinement should ensure that the scheme is free from dispersion effects. Parallel computation for the LB scheme is conducted on 30 cores to reduce computational time. Fig. 19(a) and (b) show the pressure variations ($x = 25$ m, $y = 0$) obtained from the FVRS and LB computational schemes, respectively. The two waveforms observed in Fig. 19 correspond to the separated plane wave mode and the first radial mode [22,23]. Fig. 19 shows that, although using a highly refined mesh, the LB scheme still suffers from large dissipative effects. In comparison with the 5th order FVRS, the LB scheme is inefficient at 2nd order accuracy. In fact, even with the advantage of LB scheme having optimized parallelization feature, the 5thorder FVRS running on a single core requires less computational time (9h4min versus 10h20min for the LB scheme). This demonstrates the importance of using the high order accuracy of the scheme when modeling high frequency (dispersive) waves. The effect of high order terms in LB formulations would need further investigation to determine whether better performance might be achieved when modeling HFWs. This work will be discussed in subsequent paper.

3.5. Conclusion

The lattice Boltzmann method with multiple relaxation times is used to model 1-d and 2-d water hammer test cases. For the 1-d case, it is shown that LBM gives the exact solution of pressure variation for inviscid flow. This is important since, in the literature and common usage, LBM are typically employed to solve only viscous flow and become unstable for inviscid flow test cases. In fact, the inviscid flow problem can be handled by choosing the tuning parameter (α) to be 1, and it is found that this parameter ($\sqrt{\alpha}$) represents the CFL number. For the 2-d case, the LB scheme is compared with a 5th order FV scheme based on Riemann solver. First the classical water hammer test is considered with laminar flow. It is found that the relaxation parameter s_3, which relates to the bulk viscosity, governs the dissipation mechanism of radial waves. On the other hand, the relaxation parameter s_8, which relates to the shear viscosity, governs the dissipation mechanism of

axial waves. Overall, the results show that the LB scheme is capable of modeling water hammer applications with good accuracy and performance for low frequency cases. Second, a specific high frequency test case is considered where high frequency smooth waves are injected into an infinite single pipe with a narrow frequency bandwidth such that the plane wave mode (M0) and the first radial mode (M1) are excited and become separated as they propagate. The results of this numerical investigation show that the LB scheme becomes unstable and its performance when modeling high frequency waves is significantly impaired. It is presumed that deterioration in stability and accuracy may be due to neglecting high order terms of the equivalent macroscopic equations considered during the LB numerical formulation. A more detailed analysis of the dissipation mechanism of the LB scheme when modeling high frequency acoustic waves will be discussed in a subsequent paper.

Acknowledgments

Appendix A. LBM scheme

The moment matrix for the D2Q9 scheme is:

$$M = \begin{pmatrix} 1 & 1 & 1 & 1 & 1 & 1 & 1 & 1 & 1 \\ 0 & \lambda & 0 & -\lambda & 0 & \lambda & -\lambda & -\lambda & \lambda \\ 0 & 0 & \lambda & 0 & -\lambda & \lambda & \lambda & -\lambda & -\lambda \\ -4 & -1 & -1 & -1 & -1 & 2 & 2 & 2 & 2 \\ 4 & -2 & -2 & -2 & -2 & 1 & 1 & 1 & 1 \\ 0 & -2 & 0 & 2 & 0 & 1 & -1 & -1 & 1 \\ 0 & 0 & -2 & 0 & 2 & 1 & -1 & -1 & 1 \\ 0 & 1 & -1 & 1 & -1 & 0 & 0 & 0 & 0 \\ 0 & 0 & 0 & 0 & 0 & 1 & -1 & 1 & -1 \end{pmatrix}. \quad \text{(A.1)}$$

The equilibrium values are given by:

$$\begin{cases} m_3^{eq} = \alpha \rho + \frac{3}{\lambda^2 \rho}(j_x^2 + j_y^2), & m_4^{eq} = \beta \rho - \frac{3}{\lambda^2 \rho}(j_x^2 + j_y^2), \\ m_5^{eq} = -\frac{j_x}{\lambda}, & m_6^{eq} = -\frac{j_y}{\lambda}, \\ m_7^{eq} = \frac{j_x^2 - j_y^2}{\lambda^2 \rho}, & m_8^{eq} = \frac{j_x j_y}{\lambda^2 \rho}. \end{cases} \quad \text{(A.2)}$$

The equivalent macroscopic equations [11] at order two are:

$$\frac{\partial \rho}{\partial t} + \frac{\partial j_x}{\partial x} + \frac{\partial j_y}{\partial y} = O(\Delta t^2), \quad \text{(A.3)}$$

$$\frac{\partial j_x}{\partial t} + \lambda^2 \frac{\alpha+4}{6} \frac{\partial \rho}{\partial x} + \frac{\partial}{\partial x} \frac{j_x^2}{\rho} + \frac{\partial}{\partial y} \frac{j_x j_y}{\rho}$$
$$= \lambda^2 \Delta t \left[\frac{-\alpha}{6} \left(\frac{1}{s_3} - \frac{1}{2} \right) \frac{\partial}{\partial x} \left(\frac{\partial j_x}{\partial x} + \frac{\partial j_y}{\partial y} \right) + \frac{1}{3} \left(\frac{1}{s_8} - \frac{1}{2} \right) \Delta j_x \right]$$
$$+ O(\Delta t^2), \quad \text{(A.4)}$$

$$\frac{\partial j_y}{\partial t} + \lambda^2 \frac{\alpha+4}{6} \frac{\partial \rho}{\partial y} + \frac{\partial}{\partial x} \frac{j_x j_y}{\rho} + \frac{\partial}{\partial y} \frac{j_y^2}{\rho}$$
$$= \lambda^2 \Delta t \left[\frac{-\alpha}{6} \left(\frac{1}{s_3} - \frac{1}{2} \right) \frac{\partial}{\partial y} \left(\frac{\partial j_x}{\partial x} + \frac{\partial j_y}{\partial y} \right) + \frac{1}{3} \left(\frac{1}{s_8} - \frac{1}{2} \right) \Delta j_y \right]$$
$$+ O(\Delta t^2), \quad \text{(A.5)}$$

where Δf is the Laplacian operator in space of the function f. The parameter α is linked to the sound speed $c_s = \lambda \sqrt{\frac{\alpha+4}{6}}$. The relaxation parameters s_3 and s_8 are related to the bulk ζ_0 and kinematic ν_0 viscosities such as $\zeta_0 = \frac{-\alpha \lambda^2 \Delta t}{6}(\frac{1}{s_3} - \frac{1}{2})$ and $\nu_0 = \frac{\lambda^2 \Delta t}{3}(\frac{1}{s_8} - \frac{1}{2})$, respectively (e.g. see [20]). To ensure the isotropicity of the dissipation process (ν_0), s_7 and s_8 are taken equal. At second order accuracy, the coefficient β and the relaxation rates s_4, s_5 and s_6 play no role in the hydrodynamic behavior of the model, however, they are relevant for the stability and the accuracy of the scheme [13].

Remark. Using the inverse of moment matrix M (see Eq. (A.1)), the equilibrium distribution given by Eq. (A.2) becomes in the f space:

$$f_i^{eq} = \omega_i \left[\rho + \left(3V.c_i + \frac{9}{2}(V.c_i)^2 - \frac{3}{2}|V|^2 \right) \right], \qquad i = 0, \ldots 8, \quad \text{(A.6)}$$

where weights ω_i are some fixed numbers such that $\sum_{i=0}^{8} \omega_i = 1$ and ρ, $V = (V_x, V_y)$ are respectively the density and velocity of the fluid. The truncated equilibrium Eq. (A.6), which approximate the Maxwell distribution, is used because the velocity space is discretized. This approximation comes naturally from Hermite polynomial expansion [30].

References

[1] Budinski L. Application of the LBM with adaptive grid on water hammer simulation. J Hydroinf 2016;18:687–701.

[2] Buick JM, Greated CA, Campbell DM. Lattice BGK simulation of sound waves. Europhys Lett 1998;43:235–40.

[3] Bouzidi M, Firdaous M, Lallemand P. Momentum transfer of a Boltzmann-lattice fluid with boundaries. Phys Fluids 2001;13:3452–9.

[4] Chaudhry MH. Applied hydraulic transients. 3rd ed. New York: Springer; 2014.

[5] Chen S, Doolen GD. Lattice Boltzmann method for fluid flows. Annu Rev Fluid Mech 1998;30:329–64.

[6] Chikatamarla SS, Ansumali S, Karlin IV. Entropic lattice Boltzmann models for hydrodynamics in three dimensions. Phys Rev Lett 2006;64:010201.

[7] Crouse B, Freed D, Balasubramanian G, Senthooran S, Lew P, Mongeau L. Fundamental aeroacoustics capabilities of the lattice-Boltzmann method. AIAA Paper 2006;2:006–2571.

[8] Dellar PJ. Bulk and shear viscosities in lattice Boltzmann equations. Phys Rev E 2001;64:031203.

[9] Dellar PJ. Lattice kinetic schemes for magnetohydrodynamics. J Comput Phys 2002;179:95–126.

[10] Duan HF, Lee PJ, Ghidaoui MS, Tung YK. Extended blockage detection in pipelines by using the system frequency response analysis. J Water Resour Plan Manage ASCE 2011;138:55–63.

[11] Dubois F. Une introduction au schéma de Boltzmann sur réseau. In: ESAIM: proceedings, 18; 2007. p. 181–215.

[12] Dubois F. Equivalent partial differential equations of a Boltzmann scheme. Comput Math Appl 2008;55:1441–9.

[13] Dubois F, Lallemand P, Tekitek MM. On a superconvergent lattice Boltzmann boundary scheme. Comput Math Appl 2010;59:2141.

[14] Dubois F, Lallemand P, Tekitek MM. Generalized bounce back boundary condition for the nine velocities two-dimensional lattice Boltzmann scheme. Comput Fluids 2017. doi:10.1016/j.compfluid.2017.07.001.

[15] Ghidaoui MS. On the fundamental equations of water hammer. Urban Water J 2004;1:71–83.

[16] Geier M, Schönherr M, Pasquali A, Krafczyk M. The cumulant lattice Boltzmann equation in three dimensions: theory and validation. Comput Math Appl 2015;70:507.

[17] Ginzburg I, Verhaeghe F, d'Humières D. Two-relaxation-time lattice Boltzmann scheme: about parametrization, velocity, pressure and mixed boundary conditions. Commun Comput Phys 2008;3:427–78.

[18] d'Humières D. Generalized lattice-Boltzmann equations. In: Rarefied gas dynamics: theory and simulations, 159 of AIAA progress in astronautics and astronautics; 1992. p. 450–8.

[19] Junk M, Klar A, Luo LS. Asymptotic analysis of the lattice Boltzmann equation. J Comput Phys 2005;210:676–704.

[20] Lallemand P, Luo L-S. Theory of the lattice Boltzmann method: dispersion, dissipation, isotropy, galilean invariance, and stability. Phys Rev E 2000;61:6546–62.

[21] Lee PJ, Duan HF, Ghidaoui MS, Karney B. Frequency domain analysis of pipe fluid transient behaviour. J Hydraul Res 2013;51:609–22.

[22] Louati M. In-depth study of plane wave-blockage interaction and analysis of high frequency waves behaviour in water-filled pipe systems; 2016. Doctoral dissertation. Available at: (http://lbezone.ust.hk/bib/b1618552).

[23] Louati M, Ghidaoui MS. High frequency acoustic waves in pressurized fluid in a conduit. part 1: dispersion behaviour. J Hydraul Res 2017. doi:10.1080/00221686.2017.1354931.

[24] Louati M, Ghidaoui MS. High-frequency acoustic wave properties in a water-filled pipe. Part 2: range of propagation. J Hydraul Res 2017. doi:10.1080/00221686.2017.1354934.

[25] Louati M, Ghidaoui MS. The need of high order numerical scheme for modeling dispersive high frequency acoustic waves in water-filled pipe. J Hydraul Res. in press. 2018.

[26] Louati M, Meniconi M, Ghidaoui MS, Brunone B. Experimental study of the eigenfrequency shift mechanism in blocked pipe system. J Hydraul Eng 2017:04017044. doi:10.1061/(ASCE)HY.1943-7900.0001347.

[27] Marié S, Ricot D, Sagaut P. Comparison between lattice Boltzmann method and Navier-Stokes high order schemes for computational aeroacoustics. J Comput Phys 2009;228:1056–70.

[28] Meniconi S, Duan HF, Lee PJ, Brunone B, Ghidaoui MS, Ferrante M. Experimental investigation of coupled frequency and time-domain transient test-based techniques for partial blockage detection in pipelines. J Hydraul Eng ASCE 2013;139:1033–40.

[29] Qian YH, D'Humières D, Lallemand P. Lattice BGK models for Navier-Stokes equation. Europhys Lett 1992;17:479–84.

[30] Shan XW, Yuan XF, Chen HD. Kinetic theory representation of hydrodynamics: a way beyond the Navier-Stokes equation. J Fluid Mech 2006;550: 413–441.

[31] Wang J, Wang D, Lallemand P, Luo L-S. Lattice Boltzmann simulations of thermal convective flows in two dimensions. Comput Math Appl 2013;65: 262–286.

[32] Yepez J. Quantum lattice-gas model for the burgers equation. J Stat Phys 2002;107:203–24.

[33] Wylie EB, Streeter VL, Suo L. Fluid transients in systems. NJ: Prentice Hall Englewood Cliffs; 1993.